Radiology

Quantification of Liver Fat Content with CT and MRI: State of the Art

Jitka Starekova, MD • *Diego Hernando, PhD* • *Perry J. Pickhardt, MD* • *Scott B. Reeder, MD, PhD*

From the Departments of Radiology (J.S., D.H., P.J.P., S.B.R.), Medical Physics (D.H., S.B.R.), Biomedical Engineering (S.B.R.), Medicine (S.B.R.), and Emergency Medicine (S.B.R.), University of Wisconsin, 1111 Highland Ave, Madison, WI 53705. Received November 13, 2020; revision requested December 21; revision received April 19, 2021; accepted April 26. **Address correspondence to** J.S. (e-mail: *starekova@wisc.edu*).

Supported by the National Institutes of Health (R01 DK088925, R01 DK100651, R44-EB025729, R01-DK117354), the University of Wisconsin State Economic Engagement and Development (SEED) Research Program, and GE Healthcare and Bracco Diagnostics, who provide research support to the University of Wisconsin.

Conflicts of interest are listed at the end of this article.

Radiology 2021; 301:250–262 • **https://doi.org/10.1148/radiol.2021204288** • **Content codes: GI CT MR**

Hepatic steatosis is defined as pathologically elevated liver fat content and has many underlying causes. Nonalcoholic fatty liver disease (NAFLD) is the most common chronic liver disease worldwide, with an increasing prevalence among adults and children. Abnormal liver fat accumulation has serious consequences, including cirrhosis, liver failure, and hepatocellular carcinoma. In addition, hepatic steatosis is increasingly recognized as an independent risk factor for the metabolic syndrome, type 2 diabetes, and, most important, cardiovascular mortality. During the past 2 decades, noninvasive imaging-based methods for the evaluation of hepatic steatosis have been developed and disseminated. Chemical shift–encoded MRI is now established as the most accurate and precise method for liver fat quantification. CT is important for the detection and quantification of incidental steatosis and may play an increasingly prominent role in risk stratification, particularly with the emergence of CT-based screening and artificial intelligence. Quantitative imaging methods are increasingly used for diagnostic work-up and management of steatosis, including treatment monitoring. The purpose of this state-of-the-art review is to provide an overview of recent progress and current state of the art for liver fat quantification using CT and MRI, as well as important practical considerations related to clinical implementation.

Online supplemental material is available for this article.

Online SA-CME • *See www.rsna.org/learning-center-ry*

Learning Objectives:

After reading the article and taking the test, the reader will be able to:

- Describe the clinical burden of nonalcoholic fatty liver disease
- Explain the principle of CT-based liver fat quantification, its strengths and limitations, and possible confounders that can mimic and mask coexisting steatosis
- Define MRI-based proton density fat fraction, MRI strategies that allow for accurate estimation of liver fat content, and its clinical implementation

Accreditation and Designation Statement

The RSNA is accredited by the Accreditation Council for Continuing Medical Education (ACCME) to provide continuing medical education for physicians. The RSNA designates this journal-based SA-CME activity for a maximum of 1.0 *AMA PRA Category 1 Credit*™. Physicians should claim only the credit commensurate with the extent of their participation in the activity.

Disclosure Statement

The ACCME requires that the RSNA, as an accredited provider of CME, obtain signed disclosure statements from the authors, editors, and reviewers for this activity. For this journal-based CME activity, author disclosures are listed at the end of this article.

Abnormal accumulation of liver fat, or hepatic steatosis, is a pathologic condition that is increasing in prevalence, progressive in nature, and associated with hepatic and extrahepatic complications. Development of quantitative imaging methods over the past 2 decades has produced accurate, precise, and reproducible methods to assess the severity of hepatic steatosis. Herein, we review state-of-the-art liver fat quantification using CT and MRI, including advantages and limitations, followed by a guide for their use in clinical practice.

Burden of Hepatic Steatosis and Nonalcoholic Fatty Liver Disease

In hepatic steatosis, several lipid metabolites can accumulate in the liver, including triglycerides (the majority), free fatty acids, and cholesterol (1,2). In the absence of specific causes (eg, alcohol abuse, steatogenic medications, or viral infection), the term *nonalcoholic fatty liver disease* (NAFLD) is used (3). NAFLD is the most common chronic liver disease (4), with an estimated pooled overall global prevalence of 25%, as diagnosed with imaging (US and/or CT) (4). Areas most affected include the Middle East (32%), South and North America (30% and 24%, respectively), and Asia (27%) (4).

NAFLD can occur at an early age (5) and may result in fibrosis or cirrhosis in childhood or early adulthood (5,6). The pooled mean prevalence of pediatric NAFLD is estimated to be 8% in the general population and 34% in children seen at obesity clinics (6). As for the early onset of NAFLD, additional considerations including race, ethnicity (7), and genetically inherited metabolic disorders should be considered (3,7,8). Pediatric NAFLD, however, remains generally underdiagnosed because of lack of awareness.

NAFLD represents a spectrum of disease, with the majority at one end with only "isolated" hepatic steatosis or nonalcoholic fatty liver (3). A fraction of patients with NAFLD, estimated at 20% (projected to be 27% in 2030), will develop hepatocyte injury and inflammation, representing a more aggressive subset known as nonalcoholic steatohepatitis (NASH). We note that an

Abbreviations

CSE = chemical shift encoded, MRS = MR spectroscopy, NAFLD = nonalcoholic fatty liver disease, NASH = nonalcoholic steatohepatitis, PDFF = proton density fat fraction, ROI = region of interest, SNR = signal-to-noise ratio

Summary

Noninvasive quantitative imaging is central to the detection, quantitative grading, and management of hepatic steatosis; although chemical shift–encoded MRI represents the most precise and reproducible method for liver fat quantification and surveillance, CT is playing an increasingly important role in the detection of incidentally detected steatosis and its initial grading.

Essentials

- Chemical shift–encoded (CSE) MRI has emerged as the primary clinical and research tool, providing estimates of proton density fat fraction (PDFF) as a reliable biomarker for the detection and quantification of liver fat content.
- Accurate, precise, and reproducible quantitative volumetric assessment of hepatic steatosis over the entire liver is possible within a single breath hold with CSE MRI.
- Attenuation values at unenhanced CT are linear, correlate strongly with PDFF, and offer an alternative means to quantify liver fat content.
- Postcontrast CT is less accurate in the assessment of mild hepatic steatosis but can be used for detecting moderate-to-severe steatosis (≥30% lipid fat content at histopathologic examination).
- Nonalcoholic fatty liver disease (NAFLD) is strongly associated with the metabolic syndrome and cardiovascular morbidity and mortality, warranting active research into the relationship between liver fat and these conditions; the renaming of NAFLD to metabolic associated fatty liver, or MAFLD, has recently been proposed although not yet widely adopted.

estimated 20% (projected to be 29% in 2030) of patients with NASH will develop stage F3 or F4 fibrosis (ie, advanced fibrosis and/or cirrhosis) (9).

Patients with NAFLD, particularly those with NASH, are at higher risk for adverse outcomes (3,4). NAFLD is an independent risk factor for hepatocellular carcinoma, and NASH-related cirrhosis is the second-most common indication for liver transplant in the United States (3). Moreover, NAFLD is often present in alcoholic liver disease and hepatitis C virus infection, the current leading causes for liver transplant (3,10).

Isolated steatosis, previously considered as "benign" or "simple"—misnomers that should be abandoned in our opinion—is increasingly recognized to have important clinical implications. Liver fat is strongly associated with metabolic syndrome (4) and cardiovascular diseases (3,11) and may even play a causative role in the development of type 2 diabetes (3). The prevalence of diabetes and metabolic syndrome among patients with NAFLD is estimated to be 23% and 41%, respectively (4). Nonalcoholic fatty liver is also associated with increased prevalence of coronary artery disease and atherosclerosis (odds ratio: 1.9 and 1.3, respectively) (12), and liver fat has been shown to be an independent risk factor for high-risk plaque (odds ratio: 2.1) (11). Of note, cardiovascular disease deaths associated with elevated liver fat content far exceed liver-specific mortality in patients with NAFLD: The cardiac-specific mortality among patients with NAFLD is 4.8 per 1000 person-years, which is higher than liver-specific mortality (0.77 per 1000 person-years) (4).

Finally, it is important to note that the nomenclature NAFLD may change in the near future. Due to the increasingly recognized strong association of NAFLD with metabolic diseases, renaming NAFLD to metabolic-associated fatty liver disease, or MAFLD, has been proposed (13,14). Although not yet widely accepted, the goal of the redefinition is to increase patient awareness and understanding as well as to more effectively express the underlying cause of the disease (13,14).

Detection and Diagnosis of Hepatic Steatosis

At present, nontargeted liver biopsy remains the definitive reference standard for steatosis detection and grading. Histologically, grading represents the percentage of hepatocytes containing intracellular lipid–containing vacuoles (2). According to Brunt et al (2), grade 0 (<5% hepatocytes affected) is normal, grade 1 (5%–33% hepatocytes affected) is mild, grade 2 (34%–66% hepatocytes affected) is moderate, and grade 3 (>66% hepatocytes affected) is severe. A commonly used threshold for moderate steatosis is 30% (15–17). Of note, the histopathologic thresholds are based on visual assessment, with no basis in prognosis or other clinical outcome (18). Importantly, the histopathologic grade should not be confused with MRI proton density fat fraction (PDFF, in percentage), which is an entirely different metric (19). In contrast to the former, PDFF represents a calculated signal liver fat fraction, at the voxel level at MR spectroscopy (MRS) or on a pixel-by-pixel basis in an MRI-derived parametric map (MRI PDFF map) (20).

An important limitation of liver biopsy includes its impractical nature for routine and repeat steatosis assessment (3,4). Furthermore, biopsy has high sampling variability, a fundamental limitation related to sampling of approximately just 1:50 000th of the liver; this may lead to inaccurate steatosis estimation (21,22). Last, biopsy requires sedation and is expensive (21,23).

Conversely, noninvasive imaging has witnessed substantial progress during the past 2 decades, enabling cost-effective, safe, rapid, and accurate volumetric assessment of steatosis over the entire liver (Fig 1), and is increasingly preferred as a method of choice in the clinical realm (24,25).

US: Feasibility and Limitations

US is the most common modality used for the initial evaluation of elevated liver enzymes, often related to hepatic steatosis. However, most sonographic examinations are qualitative in nature and limited in performance, particularly in obese patients, who are at highest risk of NAFLD.

Conventional US (B-mode US) facilitates estimation of steatosis severity on the basis of subjective analysis of sonographic patterns (26). With B-mode US, steatosis is typically graded as absent (score, 0), mild (score, 1; slight diffuse increase in liver echogenicity), moderate (score, 2; moderately increased liver echogenicity, slightly impaired visibility of diaphragm and the portal vein wall), or severe (score, 3; marked increased echogenicity of the liver, poor visualization of diaphragm, portal vein wall, and posterior parts of the right liver lobe) (27). Importantly,

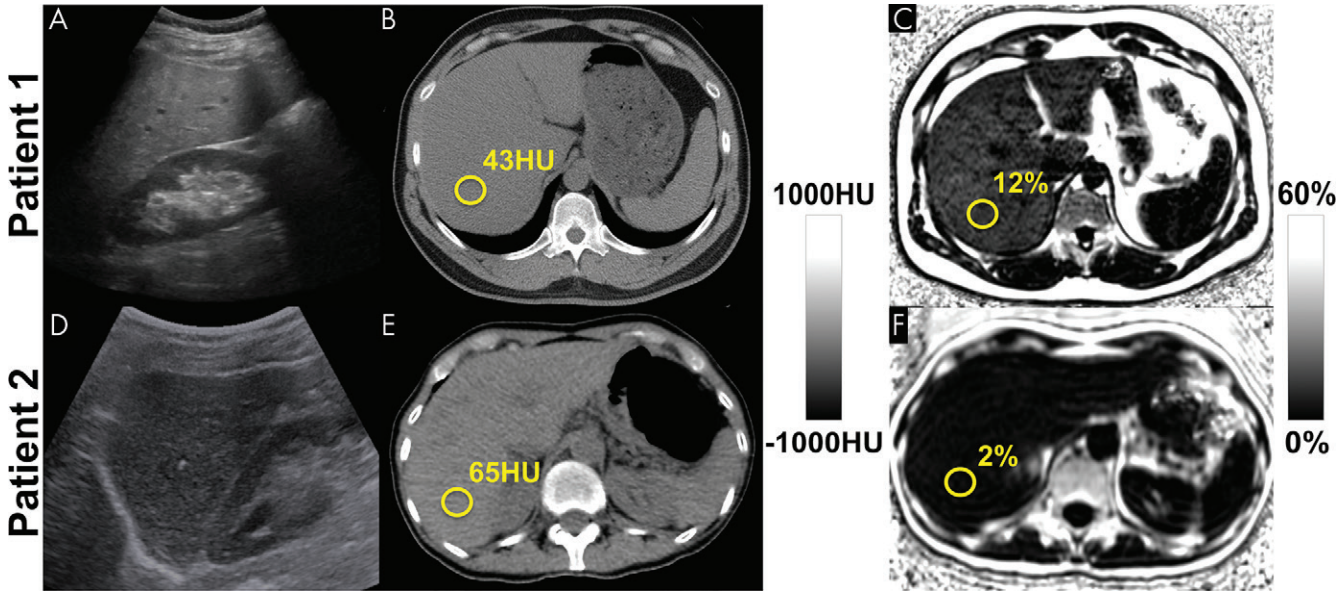

Figure 1: Among the noninvasive modalities used for quantification of liver fat, chemical shift–encoded (CSE) MRI–based proton density fat fraction (PDFF) mapping has the best combination of accuracy, precision, and reproducibility in the measurement of liver fat content. Estimation of hepatic fat content using US is based on increased echogenicity and sound attenuation and has low accuracy for detection of mild-to-moderate steatosis. Decreased x-ray attenuation (Hounsfield units) on noncontrast CT scans can be used to quantify liver fat and correlates closely and linearly with MRI PDFF. CSE MRI generates confounder-corrected volumetric quantitative maps of PDFF, a fundamental property of tissue. **(A, D)** Conventional US images, **(B, E)** noncontrast CT images, and **(C, F)** MRI PDFF maps in 44-year-old man (patient 1) with mild-to-moderate hepatic steatosis (MRI PDFF = 12%, CT attenuation = 43 HU) and 59-year-old woman (patient 2) without steatosis (MRI PDFF = 2%, CT attenuation = 65 HU).

conventional B-mode US has only moderate diagnostic performance for hepatic steatosis of 5% or greater (sensitivity, 50%–62%), may fail in obese patients or those with ascites, and is highly operator- and platform-dependent (28–30).

Considerable effort has been directed toward the development of quantitative US techniques such as attenuation and backscatter coefficient, controlled attenuation parameter, shear-wave elastography and dispersion, speed of sound, and quantitative US spectroscopy (26,31,32). The controlled attenuation parameter method, which is based on transient elastography implemented as part of the FibroScan technology (Echosens, approved by the U.S. Food and Drug Administration in 2013), is the most widely studied quantitative US approach and has shown moderate performance for the detection of hepatic steatosis for MRI PDFF of a least 5%, with reported sensitivity and specificity of 75% and 77% (cutoff, 288 dB/m) (25). A comprehensive review of controlled attenuation parameter and other quantitative US methods is beyond the scope of this article and can be found in recent publications (26,27,33,34).

Advances in quantitative US are expected to improve the accuracy and reproducibility of US-based liver fat quantification. However, the availability of numerous emerging quantitative US techniques from a large number of vendors may paradoxically hinder dissemination owing to the challenge of harmonizing methods across vendors and platforms (34).

CT and MRI

CT and MRI are cross-sectional imaging modalities capable of enabling the detection and quantification of liver fat content on the basis of different physical principles. CT exploits changes in x-ray attenuation in the presence of fat, measured in Hounsfield units (35,36). MRI exploits differences in Larmor frequencies, or chemical shift, between protons in triglycerides and those in water, providing quantitative estimates of PDFF (37).

CT Examination

CT is a widely used imaging method capable of enabling objective estimation of liver fat content. The x-ray absorption of triglycerides is lower than that of normal liver (35), leading to a decrease in attenuation with increasing fat content (Fig 2) (15,38). At unenhanced CT, mean liver attenuation for biopsy-proven absence of fat is approximately 64 HU, whereas moderate steatosis corresponds to approximately 42 HU (36). In general, unenhanced CT is superior to contrast-enhanced CT in the prediction of pathologic liver fat content determined with histopathologic examination (R^2 = 0.65 vs 0.51, respectively) (36). Iodinated contrast material increases liver attenuation, confounding and often precluding accurate quantification of liver fat content (36,39).

The sensitivity and specificity of CT for mild steatosis (cut-off values at liver biopsy, 10%–20%) is 57% and 88%; for higher-grade steatosis (cut-off values at liver biopsy, >25%), the sensitivity of CT increases to 72% and specificity to 95% (28). A threshold of 48 HU at unenhanced CT has been shown to be highly specific (100%) for moderate-to-severe steatosis (≥30%) determined at histologic examination, with a sensitivity of 54%, positive predictive value of 100%, and negative predictive value of 94% (16).

CT-based liver fat content has traditionally been evaluated using attenuation values (16,40,41), which is convenient in routine practice. A recently demonstrated linear relationship between Hounsfield unit at unenhanced CT and PDFF allows for

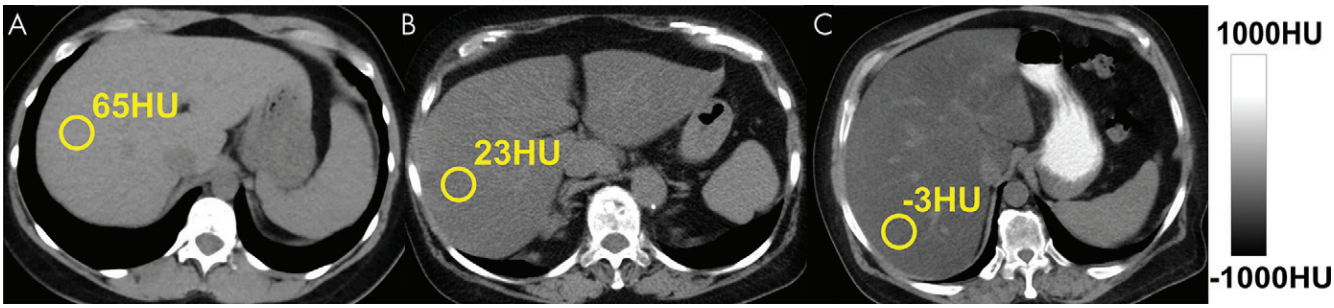

Figure 2: Triglycerides have lower x-ray absorption than normal liver parenchyma, leading to decreased CT attenuation (measured in Hounsfield units) with increasing liver fat content. Shown are three example noncontrast CT images in patients with increasing degrees of fat content. Images were obtained in **(A)** a patient with normal liver and **(B, C)** patients with moderate-to-severe (**B**) and severe (**C**) hepatic steatosis. The MRI proton density fat fraction equivalent values to 65 HU, 23 HU, and −3 HU are approximately 0.5%, 25%, and 40%, respectively.

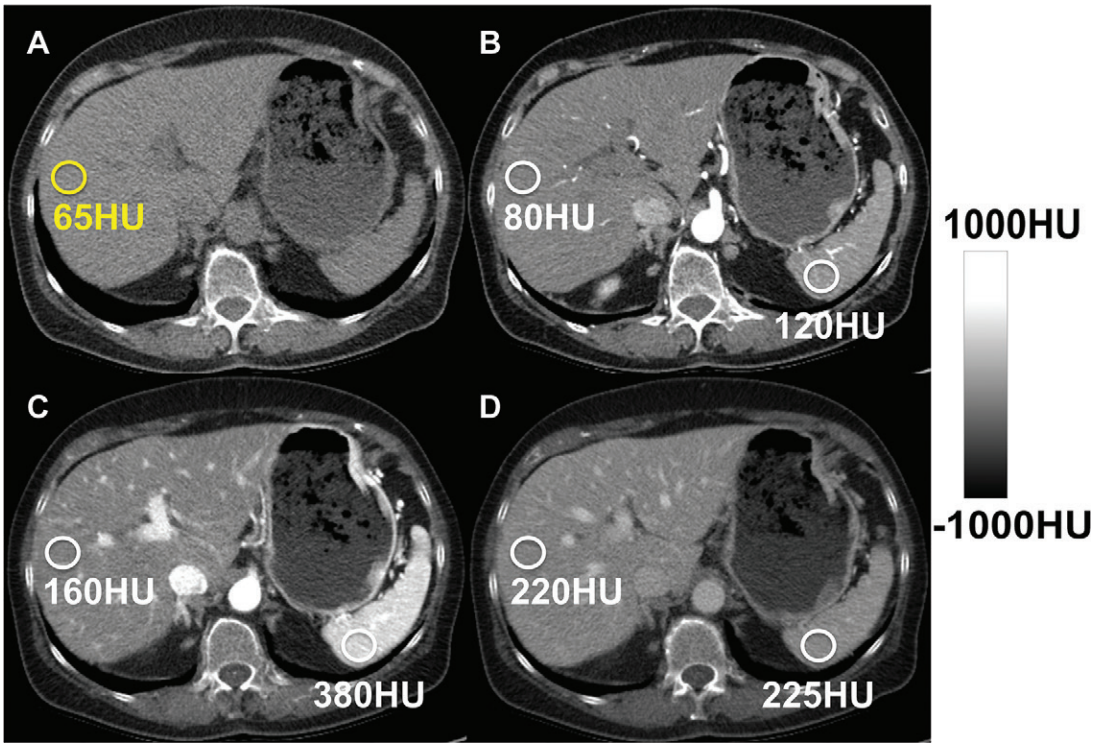

Figure 3: Hepatic steatosis can be quantified using the absolute unenhanced CT attenuation measured in Hounsfield units. Relative liver-spleen Hounsfield unit difference can be used when iodinated contrast material has been administered. An important pitfall to avoid is use of arterial phases where the spleen enhances earlier than the liver, which could be mistaken for hepatic steatosis using the spleen as the reference. CT scans obtained in a patient **(A)** before and **(B−D)** after contrast material administration in the arterial (**B**), late arterial (**C**), and portal venous (**D**) phases. No steatosis is seen on unenhanced CT scan (65 HU) (**A**). CT scans obtained in early (**B**) and late (**C**) arterial phase show liver Hounsfield unit is 40 HU and 220 HU less, respectively, than that in the spleen, mimicking steatosis. In portal venous phase (**D**), attenuation of liver and spleen is essentially equal.

CT-based liver fat content to be expressed as a PDFF-equivalent (15). Excellent linear correlation was observed between unenhanced CT Hounsfield unit and PDFF (15,38) in a phantom (r^2 = 0.986) and in clinical cases (R^2 = 0.828) (15), allowing derivation of a clinical CT-MRI conversion equation (15), as follows:

$$\text{PDFF}(\%) = -0.58 \times [\text{CT} - \text{HU}] + 38.2,$$

where HU is the Hounsfield unit. This equation applies to acquisitions performed at 120 kVp. Deviations from 120 kVp will lead to small but measurable deviations from this relationship (38). According to Equation (1), a PDFF of 0% corresponds to approximately 67 HU at unenhanced CT, and 0 HU would correspond to 38.2% PDFF (15). Similarly, unenhanced CT equivalents for PDFF-based thresholds for mild steatosis (≥5%) and moderate steatosis (≥15%) correspond to 57 HU and 40 HU, respectively. Conversion of unenhanced CT Hounsfield unit to PDFF may have both research and clinical applications, allowing harmonization of liver fat quantification across MRI and CT (Fig 2).

As noted earlier, in the setting of contrast-enhanced CT, both absolute and relative (normalized to spleen as internal reference) attenuation values have been used for steatosis

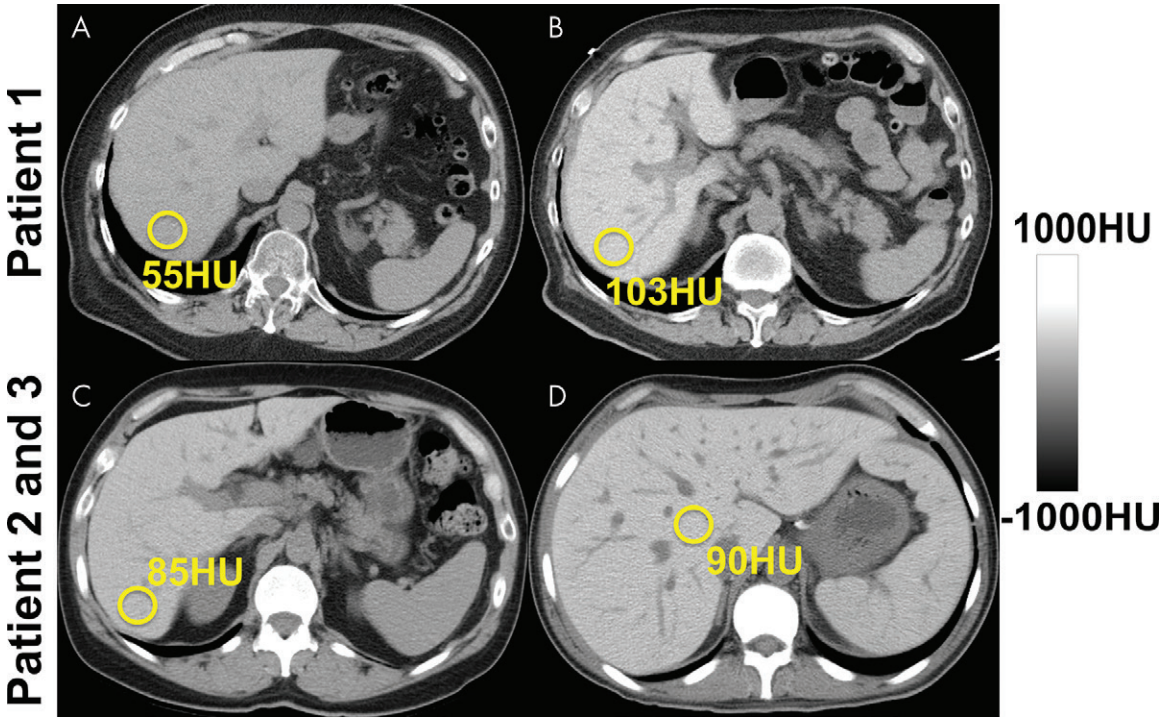

Figure 4: Detection and quantification of liver fat at CT is confounded by substances that increase the attenuation of the liver, such as amiodarone, iron, or glycogen. **(A, B)** Unenhanced CT images in a patient before (**A**) and after (**B**) long-term treatment with amiodarone. **(C, D)** CT scans obtained in patients with hereditary hemochromatosis (**C**) and transfusional hemosiderosis (**D**) show increased liver attenuation.

assessment (17,36,42) (Fig 3). Interestingly, absolute postcontrast liver attenuation measurements showed better performance (R^2 = 0.516) in the prediction of pathologic fat content determined with histologic examination than those normalized to spleen (liver-spleen Hounsfield unit difference and ratio: R^2 = 0.24 and R^2 = 0.33, respectively) (36). A liver-spleen attenuation difference of −19 HU was reported as the optimal cutoff for at least 30% steatosis at histopathologic examination (42). An important pitfall is use of the arterial phase, where the spleen enhances earlier than the liver, leading to potential misdiagnosis of steatosis (Fig 3). When possible, nonenhanced CT is best for the assessment of hepatic steatosis.

At this time, dual-energy CT has no clear advantage over simple attenuation (Hounsfield unit) measurements when intravenous contrast material is not present. Dual-energy CT material decomposition techniques enable separation of attenuation contributions from high- and low-energy photons (43). Importantly, energy versus attenuation curves, that is, "basis functions," for water and fat are very similar, making it fundamentally difficult to separate water and fat attenuation using different x-ray energies. Thus, the most likely role for dual-energy CT is to separate superimposed iodine or iron overload (43–45), which can mask the presence of steatosis at single-energy CT. Mixed results using contrast-enhanced dual-energy CT for liver fat quantification have been reported (38,45,46). Given the linear relationship of unenhanced CT to MRI PDFF, the simplest approach may be the apparent attenuation of virtual noncontrast images derived from dual-energy CT.

Clinical CT offers an important opportunity for detecting incidental steatosis and may help elucidate the natural history of NAFLD (47). However, it is important to be mindful of various pitfalls, superimposed iron (Fig 4), amiodarone (Fig 4), iodine contrast (Fig 3), glycogen overload, and hepatitis (20,36,38)—conditions that increase the attenuation of the liver and could mimic and also mask the coexisting steatosis. Of note, the effect of iron on CT attenuation is very weak and may be relevant only in moderate-to-severe iron overload (39).

Liver attenuation is also affected by beam hardening in patients with large body habitus, kilovolt peak settings, and vendor-specific filters, although these effects are small (38). Therefore, the primary diagnostic and monitoring tool for specific evaluation of hepatic steatosis should be MRI, which enables accurate and precise measurements without the use of ionizing radiation.

MRI Examinations

MRI is an imaging method rich with contrast mechanisms capable of enabling the detection and quantification of liver fat content by means of direct measurement of proton signal in water and fat (20).

Conventional qualitative methods used in the past include in-phase and opposed-phase imaging or fat-suppression methods (T1-weighted gradient-echo and T2-weighted fast spin-echo sequences). Although these methods enable qualitative assessment of steatosis, they are unsuitable for quantitative assessment as a result of multiple confounding factors (discussed later) that diminish their accuracy.

Quantitative assessment of triglycerides in the tissue can be performed using confounder-corrected CSE MRI and confounder-corrected MR spectroscopy (MRS). Both CSE MRI and MRS exploit the chemical shift between water and fat resonance

frequencies. Reduced electronic shielding of protons in water molecules, relative to protons in triglycerides, leads to a resonance frequency of water higher than that of fat, by 3.4 ppm as the relative difference between water and main methylene resonance peaks, at body temperature (20). Both MRS and CSE MRI exploit this "chemical shift" to separate water and fat proton signals (20).

If the proton MRI signals of water and fat can be separated and measured, a normalized fat signal ratio can be calculated. If the signals are proportional to the proton density of water and fat, the resulting ratio is equivalent to the PDFF (19), defined as follows: PDFF = $F/(W + F)$, where F and W are the unconfounded signals from protons within mobile triglycerides and mobile water molecules, respectively (37). PDFF is expressed as percentage (range, 0%–100%) and correlates closely to the percentage of fat estimated at histologic examination (28,37).

Accurate and reproducible estimation of PDFF using CSE MRI or MRS requires that all confounders of the MRI signal are addressed (19). For CSE MRI, confounders include T1-related bias (48,49), T2* decay (49–51), spectral complexity of fat (49,50), eddy currents (52,53), noise-related bias (48), concomitant gradients (54), and even temperature (55). In short, T1-related bias occurs when an acquisition is T1 weighted where water and fat have different T1 values; T2* decay occurs if images are acquired at different echo times and can also be amplified in the presence of iron overload. For spectral complexity of fat, only the single fat spectral peak is taken into account in conventional in-phase and opposed-phase and conventional shift-based water-fat separation methods; however, for accurate quantification, optimally proton signals from all fat spectral peaks must be considered. Noise bias results from separation and recombination of magnitude water and fat images when using chemical shift–based water-fat separation methods. Eddy currents occur as a result of rapid switching of gradients and lead to phase shifts on complex images acquired at different echo times (37). MRS-based methods must address T1-related bias, T2 decay, and J-coupling, which will depend on the type of MRS acquisition (20).

If all of the above-mentioned confounders are addressed or mitigated, both CSE MRI and MRS can provide highly accurate and precise estimates of PDFF (20,38,56,57). Excellent correlation has been observed between MRI PDFF and MRS PDFF and histopathologic examination–determined liver fat content ($r = 0.743$ [$P < .001$] and $r = 0.712$ [$P < .001$], respectively), with no clear superiority of cross-sectionally diagnostic accuracy for either MRI or MRS PDFF ($z = 0.19$, $P = .849$) (58).

With the development of MRI techniques quantifying fat in the liver, methods validating these are increasingly important (59). For this purpose, phantoms, which are experimental replicas of organs or tissues, represent a practical solution for testing and quality control of MRI-based fat quantification. Homemade fat-water phantoms have been described (60,61), although commercial phantoms (eg, Calimetrix PDFF Phantom) are now available (57,62).

MRS examination.—Proton MRS is the earliest reported method quantifying liver fat using modern MRI systems (20,63). With MRS, the proton signals of water and fat obtained from a single voxel acquired during a single breath hold (approximately 20 seconds) are depicted as separate peaks in a high-resolution spectrum (64,65). The two most commonly used methods are point-resolved spectroscopy, or PRESS, and stimulated-echo acquisition mode (STEAM) (20). Although point-resolved spectroscopy has a higher signal-to-noise ratio (SNR) than STEAM, STEAM is less affected by J-coupling and is generally preferred (66). With use of histopathologic examination as the reference standard, a recent meta-analysis reported that confounder-corrected MRS has a sensitivity of 73%–89% (compared with 73%–91% for US and 82%–97% for CT) and specificity of 92%–96% (compared with 70%–85% for US and 88%–95% for CT) (28).

To obtain estimates of MRS PDFF, a single voxel is typically placed in the right liver lobe (38), avoiding large vessels and bile ducts (20). However, the use of a small voxel (approximately 2–9 cm^3) has the same intrinsic limitation of biopsy-sampling variability (67). Multivoxel MRS can be used to cover larger volumes but increases the scanning time proportionately (minutes to hours, depending on the encoding technique and spatial coverage) (68).

Single-voxel MRS has high intra- and interexamination repeatability if performed correctly (69). However, the ability to interrogate the liver in a reproducible manner over time is an important disadvantage of MRS compared with volumetric CSE MRI methods. Furthermore, MRS analysis software is not supported by most clinical MRI systems, requiring specialized expertise for acquisition and data postprocessing and limiting its use as a clinical tool. In addition, given the limited tissue sampling of MRS, compared with volumetric CSE MRI methods, the test-retest variability of MRS is generally acknowledged as higher for MRS than for CSE MRI.

CSE MRI.—CSE MRI methods separate water and fat signal components by means of strategically sampling spoiled gradient echoes at multiple echo times (typically six echoes), usually in one repetition (70). For the calculation of PDFF, acquired MRI data must be reconstructed and postprocessed by fitting to an accurate spectral model of fat and water and corrected for the above-mentioned confounders. Magnitude- and complex-based strategies are generally used in the postprocessing and calculation of CSE MRI PDFF (37). Magnitude-based CSE MRI uses the magnitude of the gradient-echo signals (ie, discards the phase of the signals), is simpler to implement, and is more robust to phase errors such as B0 field inhomogeneities and eddy currents (52,53). However, magnitude-based methods suffer from lower SNR and limited PDFF dynamic range (0%–50%). Complex-based CSE MRI uses both magnitude and phase components of the signal and can enable measurement of the full PDFF range (0%–100%). Complex-based CSE MRI has higher SNR but is more sensitive to phase errors and can suffer from occasional water-fat swaps in the presence of inhomogeneous B0 fields (71,72). Because it is uncommon for PDFF to exceed 50%, the limited dynamic range of magnitude-based CSE MRI is only relevant for applications outside the liver (eg, bone marrow, adipose tissue). Finally, hybrid-based methods have also been implemented that combine the phase insensitivity of magnitude-based methods and the high SNR and full dynamic range of complex methods (53). Whether the CSE reconstruction

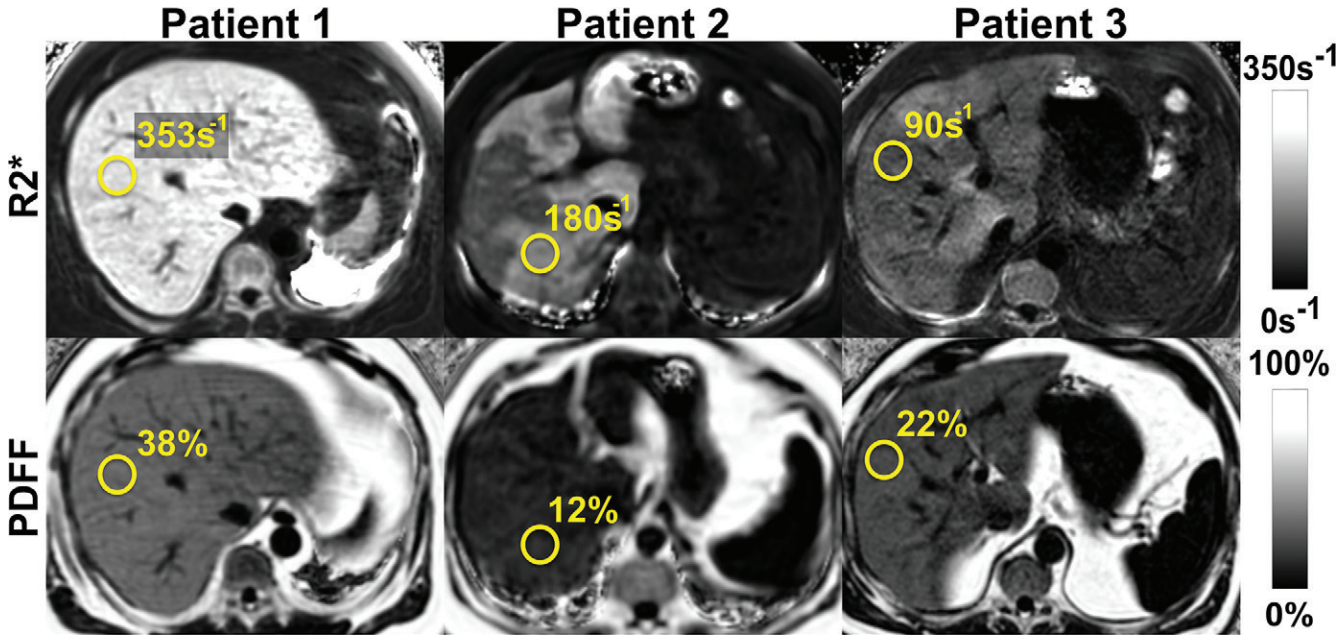

Figure 5: Chemical shift–encoded (CSE) MRI enables simultaneous estimation of both liver fat and iron deposition. Fat-corrected R2* (R2* = 1/T2*) mapping is a natural byproduct of multi-echo CSE acquisitions used for R2*-corrected proton density fat fraction (PDFF) mapping. Shown are representative MRI scans in three patients with various fat and iron levels throughout the liver.

is magnitude based, complex based, or a combination of both (hybrid method) depends on the vendor.

CSE MRI has been extensively validated in phantoms (59,73), animals (74,75), ex vivo liver tissue (76), and in clinical studies with histopathologic examination (77–79) and MRS as the reference standard (38,70). CSE MRI is considered an accurate and precise method for liver fat detection and quantification (19,24,57,58,78). CSE MRI PDFF has linear correlation with MRS PDFF (R^2 = 0.96), and it has coefficient of reproducibility and repeatability of 4.1% and 3.0%, respectively (57). Furthermore, MRI PDFF is highly reproducible across scanner platforms, manufacturers, field strengths, and imaging centers (57,80). This is particularly important for standardization and widespread dissemination of PDFF as a clinically accepted biomarker. Even though fat percentage estimated with histopathologic examination and PDFF are not interchangeable, they correlate strongly (58,78).

CSE MRI can be performed within a single breath hold and can provide near real-time PDFF map reconstruction (37) over the entire liver in approximately 15–20 seconds. Complex-based CSE MRI was first approved by the U.S. Food and Drug Administration in 2011 and is now available from all major MRI vendors for the purpose of tissue fat quantification (81), leading to widespread availability. Importantly, MRI PDFF is increasingly accepted as the most optimal method, among the invasive or noninvasive methods, for quantifying liver fat content—even overperforming biopsy (22,57,78,82). Indeed, the ability to interrogate the entire liver avoids sampling limitations of biopsy and also MRS. This is an important advantage for longitudinal studies or treatment monitoring, especially if multiple sites or scanner platforms are used. Sampling of the entire liver allows for precise co-localization of PDFF measurements from volumetric data sets acquired at different time points.

Furthermore, confounder-corrected CSE MRI also allows for simultaneous assessment of iron deposition. Iron is a paramagnetic substance and thus shortens the T2* (ie, increases the relaxation rate R2* as R2* = 1/T2*) and leads to signal loss with increasing echo time (83). Conversely, concomitant liver steatosis may mask the R2* signal decay in the liver and confound the interpretation. By means of simultaneous estimation of PDFF and R2*, CSE MRI provides fat-corrected R2* maps that enable quantification of the liver independently of the presence of fat (20,83). In contrast to other imaging methods such as CT or US, CSE MRI is thus an optimal imaging solution for coexisting fat and iron deposition in the liver (Fig 5). Coexisting fat and iron is relevant in conditions such as viral hepatitis, hepatocellular carcinoma, hemochromatosis, and hemosiderosis (83).

In many clinical scenarios, detection and quantification of either liver fat or liver iron overload is the only clinical indication for MRI, opening the opportunity for a reduced-fee abbreviated MRI protocol. Pooler et al (81) reported their experience using a rapid fat and iron MRI protocol that could be completed in as little as 3 minutes of table time. This rapid protocol includes a localizer, single-breath-hold, CSE MRI sequence providing PDFF and R2* maps and a rapid T2-weighted anatomic survey (81). In the United States, such an abbreviated examination can be appropriately billed to Medicare and/or Medicaid as a "limited" examination with modifier 52, reducing the charge by approximately 50%—which is equal to that of abdominal US (84).

Manual CT- and MRI-based Assessment of Liver Fat

Currently, there is no consensus on a standardized approach to measuring liver fat with manually drawn regions of interest (ROIs). Several standardized approaches have been proposed (85–87). Because a heterogeneous pattern of steatosis has been reported in up to 60% of patients with NAFLD (88), the place-

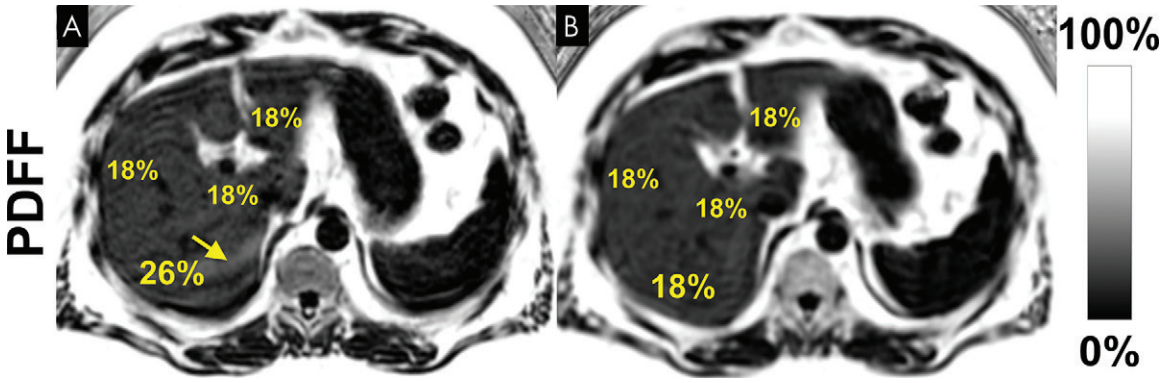

Figure 6: Motion-related ghosting from adipose tissue into the liver can lead to substantial bias and variability of proton density fat fraction (PDFF) measurements. Although three-dimensional chemical shift–encoded (CSE) MRI acquisitions are relatively short (approximately 15–20 seconds), many patients are unable to hold their breath even for this modest acquisition time. PDFF maps acquired using three-dimensional CSE MRI in the same patient during **(A)** free-breathing and **(B)** breath-hold. Scan obtained during free breathing shows artifactually increased PDFF value due to ghosting artifact from adipose tissue (arrow in **A**). .

ment of a single ROI is unlikely to be sufficient to correctly estimate the true severity of liver fat. Although placement of largest-fit-possible ROIs in all nine Couinaud hepatic segments was shown to be the most reproducible and repeatable method (87), it is time consuming and thus difficult for clinical practice. Therefore, placement of one large single-section ROI in the anterior, posterior, medial, and lateral segments of the liver, avoiding bigger vessels and bile ducts, has been proposed as an acceptable alternative (87). Future artificial intelligence–based segmentation algorithms hold promise for accurate and automated segmentation of the liver and are anticipated to lead to standardized strategies for MRI and CT analysis of liver fat.

Future Trends

Automated CT- and MRI-based Assessment of Liver Fat

Automated assessment of CT liver Hounsfield unit values and MRI PDFF maps has emerged using deep learning–based algorithms (Fig E1 [online]) for liver fat quantification (89–95). Fully automated liver segmentation may increase objectivity and reproducibility, avoiding bias introduced by human analysts (89). Several approaches have been proposed, including automated ROI extraction (90) and automated mean volumetric whole-liver attenuation using deep learning–based algorithms (89,93,94). Of note, deep learning algorithms allow for automated liver fat quantification even with incomplete coverage of the liver, such as with chest CT (91). Promising results have been shown with high correlation of automated and manually performed CT Hounsfield unit and MRI PDFF measurements (89,93). However, further refinement and evaluation of automated PDFF analysis methods is still required (Table E1 [online]). Small systematic differences observed in mean attenuation between automated and manual methods are likely due to inclusion of vessels with most automated techniques (89,91,93). Furthermore, the presence of large liver lesions or surgically altered livers are important unsolved challenges (93,94). Finally, emerging work has demonstrated that ROI-based PDFF analyses should use the median, rather than the mean, estimator (ie, average) for unbiased PDFF quantification. Asymmetric noise statistics on PDFF maps can lead to SNR-dependent bias if the mean, rather than median, PDFF value is used (96). Overall, automated algorithms are promising for rapid and objective measurement of liver fat, particularly for large cohort studies.

Respiratory Motion Mitigation with CSE MRI

Although commercially available (Table E2 [online]) CSE MRI acquisitions are short, many patients are unable to hold their breath for even a modest acquisition time. Unfortunately, even mild motion-related ghosting from adipose tissue into the liver can lead to bias and variability in PDFF (Fig 6).

To address this challenge, a variety of free-breathing strategies have been recently proposed (97–100). The use of navigator-based free-breathing acquisitions in combination with Cartesian-based complex-based CSE MRI is effective (98), although residual artifacts may remain—especially with irregular breathing. Alternatively, non-Cartesian methods (eg, radial-based methods) are showing promising results (99,101), although the reconstruction algorithms needed for these approaches are considerably more complex and radial-based methods suffer from persistent motion artifacts, especially with associated R2* maps. Development of non-Cartesian CSE MRI methods is an active area of research, although its translation to clinical practice remains uncertain at this time.

Recently, a Cartesian-based two-dimensional sequential "single-shot" CSE MRI approach has been proposed to address motion-related artifacts due to breathing (102). Exploiting a temporal footprint of approximately 0.5–1 second per section, this single-shot strategy freezes all respiratory motion. In this way, respiratory motion–related artifacts and the associated errors from aliased adipose tissue are avoided entirely. The main disadvantage of this strategy is the use of low flip angles, typically 5° at 1.5 T and 3° at 3.0 T, which is necessary to maintain proton-density weighting and avoid T1-related bias (100,102). Low flip angles in combination with short repetition times leads to low SNR (Fig 7). Recently, Zhao et al (100) addressed this limitation using a non-steady-state approach with Cartesian-based centric-encoding

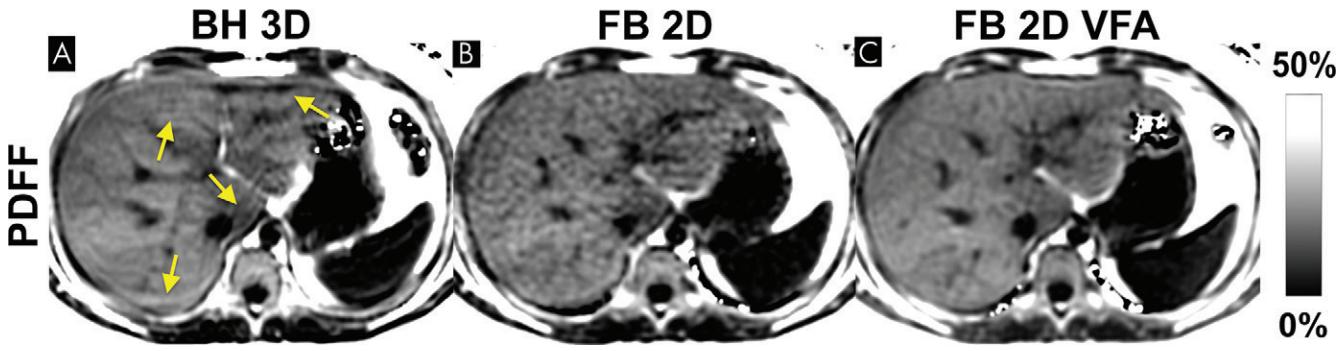

Figure 7: Free-breathing (FB) two-dimensional (2D) sequential chemical shift–encoded (CSE) MRI with centric encoding and variable flip angle (VFA) strategy is a promising technique that can mitigate respiratory motion while achieving high signal-to-noise ratio (SNR). Example proton density fat fraction (PDFF) maps using breath holding (BH) and free breathing are shown. **(A)** Three-dimensional (3D) multi-echo spoiled gradient-echo CSE MRI provides good SNR performance, but reliable breath holding is necessary to avoid motion-related artifacts that can occur even during breath holding (arrows). **(B)** Free-breathing two-dimensional CSE MRI freezes respiratory motion by using a very short temporal window, at the expense of lower SNR due to the use of low flip angles needed to avoid T1-related bias. **(C)** In contrast, a recently proposed variable flip angle sequential approach shows promise to avoid breathing artifacts and T1 bias while achieving high SNR performance (101).

and a variable flip angle strategy to maintain motion robustness while achieving high SNR performance (Fig 7).

Acceleration of MRI for Fat Liver Quantification

On the basis of recent developments, advanced methods including compressed sensing and MR fingerprinting may also enable liver fat quantification (103–105). Compressed sensing reconstruction allows reconstruction of the MRI scans using fewer phase encodes and thus shortens acquisition time (103,104), whereas fingerprinting allows for direct measurements of tissue properties and relaxation parameters (105). In fingerprinting, MRI settings and parameters deliberately vary during the data acquisition to generate a unique signal pattern or "fingerprint." These are then compared and matched to samples from a dictionary of signal patterns generated using Bloch equation simulations. Once matched, the tissue properties used for generation of a fingerprint are identified and depicted as pixel-wise maps (105).

Setting Up Clinically Meaningful PDFF Thresholds

There remains an unmet need to define PDFF thresholds that can help identify clinically meaningful stages of disease. In the Dallas Heart Study (106), a threshold of 5.56% was identified as the 95th percentile threshold in a cohort with no risk factors for liver disease. In a weight loss surgery study (107), 5% and 15% MRI PDFF thresholds have been proposed for detection and differentiation between none-to-mild and mild and/or moderate-to-severe steatosis, respectively. A recent study by Rehm et al (108) in adolescent girls identified an MRI PDFF threshold of 3.0% as predictive of metabolic syndrome. Another pediatric study (109) suggested an MRS PDFF threshold of 6.0% (sensitivity, 93%; specificity, 96%) and MRI PDFF threshold of 3.5% (sensitivity, 89%; specificity, 88%) as diagnostic for NAFLD. In summary, we propose that until definitive studies are performed, PDFF thresholds for mild, moderate, and severe steatosis should be considered at 5%, 15%, and 25%, respectively. On the basis of the CT-MRI calibration in Equation (1) (15), this corresponds to CT attenuation thresholds of 57 HU, 40 HU, and 23 HU for mild, moderate, and severe steatosis, respectively, for a CT energy of 120 kVp.

Finally, an important question is the clinically meaningful reduction of liver fat over time, particularly for the drug development in NASH clinical trials or other intervention (81). In a randomized clinical trial with biopsy-proven NASH, absolute reduction of −4.1% MRI PDFF and a relative reduction (percentage change) of −29% of the baseline MRI PDFF value over 24 weeks were shown to be associated with a histologic response in NASH (defined as two-point improvement in the NAFLD activity score) (110). Further studies are needed to establish meaningful cutoffs for liver fat reduction that, if maintained over a certain period of time, would lead to either reversal of NASH or improvement in fibrosis grade.

Clinical Implementations of Imaging Methods

The utility of imaging methods used for the severity assessment of hepatic steatosis is crucial. Moreover, given the high prevalence of hepatic steatosis, it is a common incidental finding at cross-sectional imaging. This provides a unique opportunity to report and grade the severity of steatosis to initiate lifestyle modifications or other interventions. Practice guidance statements from the American Association for the Study of Liver Diseases recommend the following for incidentally detected steatosis at imaging: *(a)* Patients with abnormal liver function tests or signs attributable to liver disease should be evaluated as suspected for NAFLD and approached accordingly and *(b)* patients with normal liver function tests should be assessed for metabolic risk factors such as obesity, dyslipidemia, or diabetes mellitus or for other alternative causes for steatosis such as excessive alcohol consumption or possibly medication induced (3).

In patients with abnormal liver function tests or incidental findings of hepatic steatosis at imaging and high clinical suspicion for NAFLD, a rapid MRI protocol targeted for liver fat quantification is the method of choice for estimating the severity of steatosis (Fig 8). Optional MRI elastography might be added to assess stiffnesses of liver tissue and fibrosis presence. If the probability of having NAFLD is lower, but steatosis cannot be excluded, an extended liver protocol should be considered.

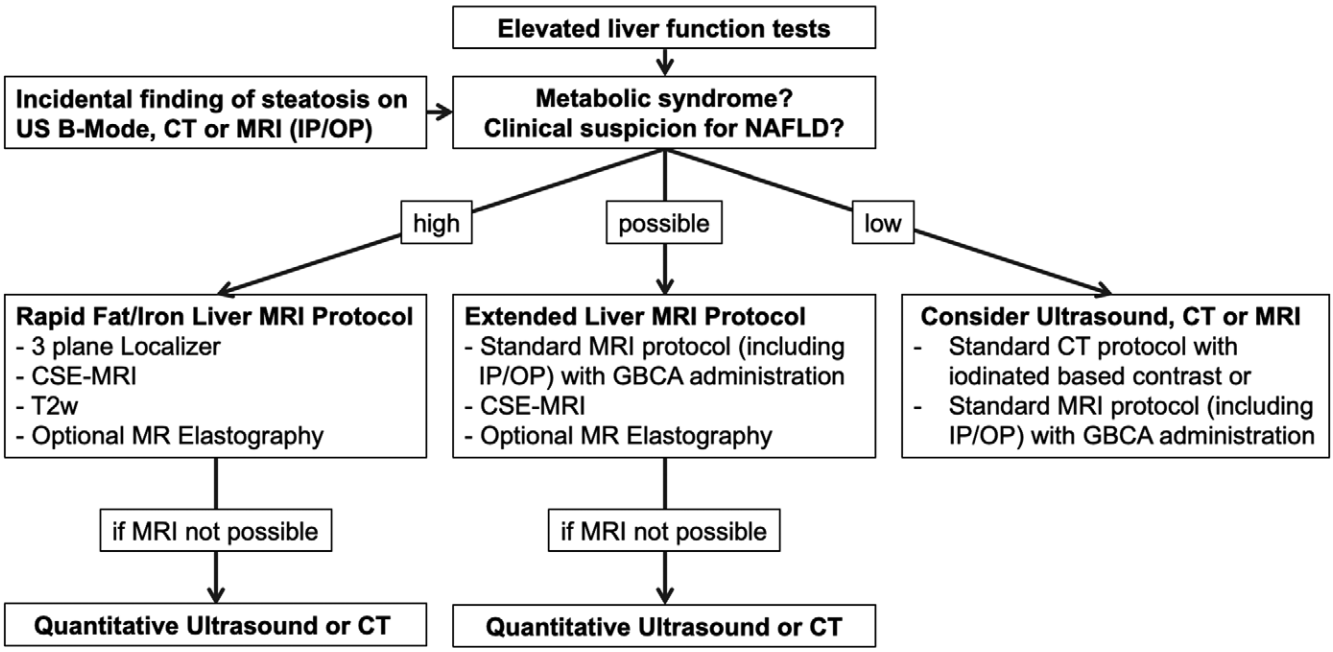

Figure 8: Flow chart shows diagnostic imaging work-up for hepatic steatosis and nonalcoholic fatty liver disease (NAFLD). In patients with abnormal liver function tests or incidental findings of hepatic steatosis at imaging and high clinical suspicion for NAFLD, a rapid MRI protocol targeted for liver fat quantification is the method of choice to estimate steatosis severity. MRI elastography might be added to assess stiffnesses of liver tissue and fibrosis presence. If the probability of having NAFLD is lower, but steatosis cannot be excluded, an extended liver protocol should be considered. CSE-MRI = chemical shift–encoded MRI, GBCA = gadolinium-based contrast agent, IP/OP = in-phase and opposed-phase imaging, T2w = T2-weighted imaging.

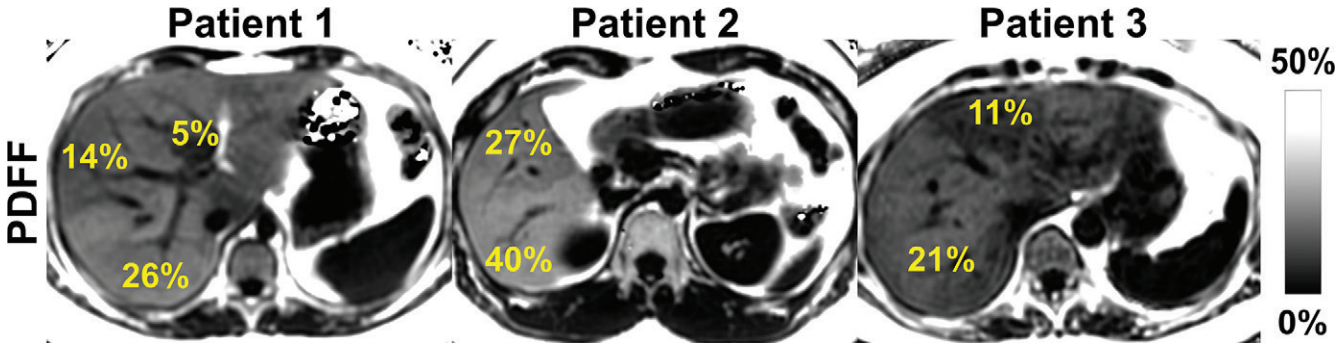

Figure 9: Chemical shift–encoded (CSE) MRI enables assessment of fat content over the entire liver, unlike MR spectroscopy and biopsy, which sample small regions of tissue and provide no information about the spatial variability of steatosis.. Shown are three-dimensional CSE MRI proton density fat fraction (PDFF) maps in three different patients with heterogeneous pattern of steatosis.

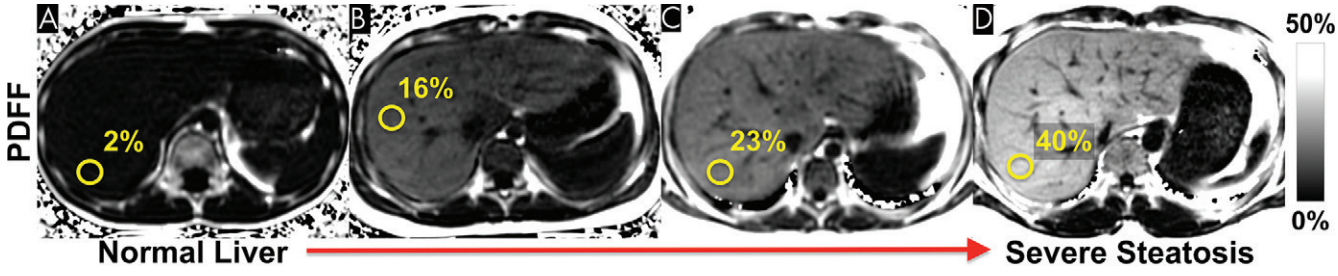

Figure 10: Nonalcoholic fatty liver disease can occur at an early age. Chemical shift–encoded (CSE) MRI allows reliable noninvasive quantification of liver fat content in children. These examples show representative proton density fat fraction (PDFF) maps obtained with CSE MRI within a single breath hold in **(A)** an 11-year-old boy with normal (<5%) liver fat content, **(B)** a 12-year-old boy with moderate steatosis, **(C)** an 11-year-old boy with moderate-to-severe steatosis, and **(D)** a 27-year-old man with severe steatosis.

CT Examination

Unenhanced CT enables reliable identification of patients with moderate-to-severe steatosis (16). Increases in the use of CT for screening lung or colorectal cancer raise the opportunity for opportunistic screening of hepatic steatosis (40,111,112). Furthermore, given that hundreds of millions of CT scans are obtained annually worldwide, CT-based liver fat quantification has great potential as a possible prognostic biomarker (111). Last, due to low diagnostic performance in mild steatosis, potential risk of ionized radiation, and other limitations of CT described earlier, CT is considered unsuitable for primary diagnosis or monitoring of hepatic steatosis. For this purpose, CSE MRI should be considered the method of choice (Fig 8).

CSE MRI

Given the subjective nature of semiquantitative evaluation of biopsy samples, which has high intra- and interobserver variability, the heterogeneous character of steatosis (Fig 9), and sampling limitations of biopsy and MRS, CSE MRI has the best combination of accuracy, precision, and reproducibility for quantification of PDFF as a biomarker of steatosis (20,22,38,78,82).

PDFF is thus a useful surrogate for liver biopsy in the diagnosis and assessment of treatment response and has even shown to be more sensitive to changes in liver fat than histologic examination (78,113). As a result, PDFF has been increasingly implemented in clinical and drug discovery trials (113–115) and will likely have increasing impact on future clinical trial design (25).

PDFF is also a valuable biomarker for preoperative risk assessment (82). Hepatic steatosis is an independent predictor of perioperative complications in liver resection (116). Furthermore, steatotic donor livers are associated with poor graft function and decreased survival (117).

Finally, CSE MRI is the method of choice for liver fat quantification in the pediatric population (Fig 10), as it has been shown to be a feasible noninvasive alternative to liver biopsy (108,109).

Conclusion

During the past 2 decades, CT and MRI have been increasingly used for the evaluation of hepatic steatosis, providing an objective measurement of liver fat content. CT has utility for detection and risk stratification, particularly using artificial intelligence–based evaluation. Given the limitations of biopsy and other imaging methods, chemical shift–encoded (CSE) MRI has emerged as the primary tool for liver fat quantification. CSE MRI–derived proton density fat fraction is an accurate, precise, and reproducible marker of hepatic steatosis and is well positioned to transform the design of diagnostic strategies and clinical trials for nonalcoholic fatty liver disease. Further advances in MRI, CT, and US are expected, including continued improvements in robustness to breathing artifacts, as well as accuracy, precision, reproducibility, cost, and access to these important biomarkers of liver fat.

Disclosures of Conflicts of Interest: J.S. disclosed no relevant relationships. **D.H.** is a cofounder of Calimetrix. **P.J.P.** is a paid consultant for Zebra and Bracco; has stock/stock options in SHINE and Elucent. **S.B.R.** is a Romnes Faculty Fellow and has received an award provided by the University of Wisconsin-Madison Office of the Vice Chancellor for Research and Graduate Education with funding from the Wisconsin Alumni Research Foundation; is a cofounder of Calimetrix.

References

1. Alkhouri N, Dixon LJ, Feldstein AE. Lipotoxicity in nonalcoholic fatty liver disease: not all lipids are created equal. Expert Rev Gastroenterol Hepatol 2009;3(4):445–451.
2. Brunt EM, Janney CG, Di Bisceglie AM, Neuschwander-Tetri BA, Bacon BR. Nonalcoholic steatohepatitis: a proposal for grading and staging the histological lesions. Am J Gastroenterol 1999;94(9):2467–2474.
3. Chalasani N, Younossi Z, Lavine JE, et al. The diagnosis and management of nonalcoholic fatty liver disease: Practice guidance from the American Association for the Study of Liver Diseases. Hepatology 2018;67(1):328–357.
4. Younossi ZM, Koenig AB, Abdelatif D, Fazel Y, Henry L, Wymer M. Global epidemiology of nonalcoholic fatty liver disease-Meta-analytic assessment of prevalence, incidence, and outcomes. Hepatology 2016;64(1):73–84.
5. Schwimmer JB, Deutsch R, Kahen T, Lavine JE, Stanley C, Behling C. Prevalence of fatty liver in children and adolescents. Pediatrics 2006;118(4):1388–1393.
6. Anderson EL, Howe LD, Jones HE, Higgins JPT, Lawlor DA, Fraser A. The prevalence of non-alcoholic fatty liver disease in children and adolescents: A systematic review and meta-analysis. PLoS One 2015;10(10):e0140908.
7. Betancourt-Garcia MM, Arguelles A, Montes J, Hernandez A, Singh M, Forse RA. Pediatric Nonalcoholic Fatty Liver Disease: the Rise of a Lethal Disease Among Mexican American Hispanic Children. Obes Surg 2017;27(1):236–244.
8. Schwimmer JB, Celedon MA, Lavine JE, et al. Heritability of nonalcoholic fatty liver disease. Gastroenterology 2009;136(5):1585–1592.
9. Estes C, Razavi H, Loomba R, Younossi Z, Sanyal AJ. Modeling the epidemic of nonalcoholic fatty liver disease demonstrates an exponential increase in burden of disease. Hepatology 2018;67(1):123–133.
10. Adinolfi LE, Gambardella M, Andreana A, Tripodi MF, Utili R, Ruggiero G. Steatosis accelerates the progression of liver damage of chronic hepatitis C patients and correlates with specific HCV genotype and visceral obesity. Hepatology 2001;33(6):1358–1364.
11. Puchner SB, Lu MT, Mayrhofer T, et al. High-risk coronary plaque at coronary CT angiography is associated with nonalcoholic fatty liver disease, independent of coronary plaque and stenosis burden: results from the ROMICAT II trial. Radiology 2015;274(3):693–701.
12. Wu S, Wu F, Ding Y, Hou J, Bi J, Zhang Z. Association of non-alcoholic fatty liver disease with major adverse cardiovascular events: A systematic review and meta-analysis. Sci Rep 2016;6:33386.
13. Fouad Y, Waked I, Bollipo S, Gomaa A, Ajlouni Y, Attia D. What's in a name? Renaming 'NAFLD' to 'MAFLD'. Liver Int 2020;40(6):1254–1261.
14. Eslam M, Sanyal AJ, George J; International Consensus Panel. MAFLD: A Consensus-Driven Proposed Nomenclature for Metabolic Associated Fatty Liver Disease. Gastroenterology 2020;158(7):1999–2014.e1.
15. Pickhardt PJ, Graffy PM, Reeder SB, Hernando D, Li K. Quantification of liver fat content with unenhanced MDCT: Phantom and clinical correlation with MRI proton density fat fraction. AJR Am J Roentgenol 2018;211(3):W151–W157.
16. Pickhardt PJ, Park SH, Hahn L, Lee SG, Bae KT, Yu ES. Specificity of unenhanced CT for non-invasive diagnosis of hepatic steatosis: implications for the investigation of the natural history of incidental steatosis. Eur Radiol 2012;22(5):1075–1082.
17. Park SH, Kim PN, Kim KW, et al. Macrovesicular hepatic steatosis in living liver donors: use of CT for quantitative and qualitative assessment. Radiology 2006;239(1):105–112.
18. Ikura Y. Transitions of histopathologic criteria for diagnosis of nonalcoholic fatty liver disease during the last three decades. World J Hepatol 2014;6(12):894–900.
19. Reeder SB, Hu HH, Sirlin CB. Proton density fat-fraction: a standardized MR-based biomarker of tissue fat concentration. J Magn Reson Imaging 2012;36(5):1011–1014.
20. Reeder SB, Cruite I, Hamilton G, Sirlin CB. Quantitative assessment of liver fat with magnetic resonance imaging and spectroscopy. J Magn Reson Imaging 2011;34(4):729–749.
21. Tapper EB, Lok ASF. Use of Liver Imaging and Biopsy in Clinical Practice. N Engl J Med 2017;377(8):756–768.
22. Ratziu V, Charlotte F, Heurtier A, et al. Sampling variability of liver biopsy in nonalcoholic fatty liver disease. Gastroenterology 2005;128(7):1898–1906.
23. Boyd A, Cain O, Chauhan A, Webb GJ. Medical liver biopsy: background, indications, procedure and histopathology. Frontline Gastroenterol 2020;11(1):40–47.
24. Parente DB, Rodrigues RS, Paiva FF, et al. Is MR spectroscopy really the best MR-based method for the evaluation of fatty liver in diabetic patients in clinical practice? PLoS One 2014;9(11):e112574.

25. Caussy C, Reeder SB, Sirlin CB, Loomba R. Noninvasive, Quantitative Assessment of Liver Fat by MRI-PDFF as an Endpoint in NASH Trials. Hepatology 2018;68(2):763–772.
26. Ozturk A, Grajo JR, Gee MS, et al. Quantitative Hepatic Fat Quantification in Non-alcoholic Fatty Liver Disease Using Ultrasound-Based Techniques: A Review of Literature and Their Diagnostic Performance. Ultrasound Med Biol 2018;44(12):2461–2475.
27. Ferraioli G, Soares Monteiro LB. Ultrasound-based techniques for the diagnosis of liver steatosis. World J Gastroenterol 2019;25(40):6053–6062.
28. Bohte AE, van Werven JR, Bipat S, Stoker J. The diagnostic accuracy of US, CT, MRI and 1H-MRS for the evaluation of hepatic steatosis compared with liver biopsy: a meta-analysis. Eur Radiol 2011;21(1):87–97.
29. Lee SS, Park SH, Kim HJ, et al. Non-invasive assessment of hepatic steatosis: prospective comparison of the accuracy of imaging examinations. J Hepatol 2010;52(4):579–585.
30. Saadeh S, Younossi ZM, Remer EM, et al. The utility of radiological imaging in nonalcoholic fatty liver disease. Gastroenterology 2002;123(3):745–750.
31. Paige JS, Bernstein GS, Heba E, et al. A pilot comparative study of quantitative ultrasound, conventional ultrasound, and MRI for predicting histology-determined steatosis grade in adult nonalcoholic fatty liver disease. AJR Am J Roentgenol 2017;208(5):W168–W177.
32. Shin J, Kim MJ, Shin HJ, et al. Quick assessment with controlled attenuation parameter for hepatic steatosis in children based on MRI-PDFF as the gold standard. BMC Pediatr 2019;19(1):112.
33. Han A, Byra M, Heba E, et al. Noninvasive diagnosis of nonalcoholic fatty liver disease and quantification of liver fat with radiofrequency ultrasound data using one-dimensional convolutional neural networks. Radiology 2020;295(2):342–350.
34. Pirmoazen AM, Khurana A, El Kaffas A, Kamaya A. Quantitative ultrasound approaches for diagnosis and monitoring hepatic steatosis in nonalcoholic fatty liver disease. Theranostics 2020;10(9):4277–4289.
35. Bydder GM, Chapman RWG, Harry D, Bassan L, Sherlock S, Kreel L. Computed tomography attenuation values in fatty liver. J Comput Tomogr 1981;5(1):33–35.
36. Kodama Y, Ng CS, Wu TT, et al. Comparison of CT methods for determining the fat content of the liver. AJR Am J Roentgenol 2007;188(5):1307–1312.
37. Reeder SB, Sirlin CB. Quantification of liver fat with magnetic resonance imaging. Magn Reson Imaging Clin N Am 2010;18(3):337–357, ix.
38. Kramer H, Pickhardt PJ, Kliewer MA, et al. Accuracy of liver fat quantification with advanced CT, MRI, and ultrasound techniques: Prospective comparison with MR spectroscopy. AJR Am J Roentgenol 2017;208(1):92–100.
39. Fischer MA, Reiner CS, Raptis D, et al. Quantification of liver iron content with CT-added value of dual-energy. Eur Radiol 2011;21(8):1727–1732.
40. Boyce CJ, Pickhardt PJ, Kim DH, et al. Hepatic steatosis (fatty liver disease) in asymptomatic adults identified by unenhanced low-dose CT. AJR Am J Roentgenol 2010;194(3):623–628.
41. Pickhardt PJ, Jee Y, O'Connor SD, del Rio AM. Visceral adiposity and hepatic steatosis at abdominal CT: association with the metabolic syndrome. AJR Am J Roentgenol 2012;198(5):1100–1107.
42. Kim DY, Park SH, Lee SS, et al. Contrast-enhanced computed tomography for the diagnosis of fatty liver: prospective study with same-day biopsy used as the reference standard. Eur Radiol 2010;20(2):359–366.
43. Fischer MA, Gnannt R, Raptis D, et al. Quantification of liver fat in the presence of iron and iodine: an ex-vivo dual-energy CT study. Invest Radiol 2011;46(6):351–358.
44. Ma J, Song ZQ, Yan FH. Separation of hepatic iron and fat by dual-source dual-energy computed tomography based on material decomposition: an animal study. PLoS One 2014;9(10):e110964.
45. Artz NS, Hines CDG, Brunner ST, et al. Quantification of hepatic steatosis with dual-energy computed tomography: comparison with tissue reference standards and quantitative magnetic resonance imaging in the ob/ob mouse. Invest Radiol 2012;47(10):603–610.
46. Hyodo T, Hori M, Lamb P, et al. Multimaterial Decomposition Algorithm for the Quantification of Liver Fat Content by Using Fast-Kilovolt-Peak Switching Dual-Energy CT: Experimental Validation. Radiology 2017;282(2):381–389.
47. Pickhardt PJ, Hahn L, Muñoz del Rio A, Park SH, Reeder SB, Said A. Natural history of hepatic steatosis: observed outcomes for subsequent liver and cardiovascular complications. AJR Am J Roentgenol 2014;202(4):752–758.
48. Liu CY, McKenzie CA, Yu H, Brittain JH, Reeder SB. Fat quantification with IDEAL gradient echo imaging: correction of bias from T(1) and noise. Magn Reson Med 2007;58(2):354–364.
49. Bydder M, Yokoo T, Hamilton G, et al. Relaxation effects in the quantification of fat using gradient echo imaging. Magn Reson Imaging 2008;26(3):347–359.
50. Yu H, McKenzie CA, Shimakawa A, et al. Multiecho reconstruction for simultaneous water-fat decomposition and T2* estimation. J Magn Reson Imaging 2007;26(4):1153–1161.
51. Yu H, Shimakawa A, McKenzie CA, Brodsky E, Brittain JH, Reeder SB. Multiecho water-fat separation and simultaneous R2* estimation with multifrequency fat spectrum modeling. Magn Reson Med 2008;60(5):1122–1134.
52. Hernando D, Hines CDG, Yu H, Reeder SB. Addressing phase errors in fat-water imaging using a mixed magnitude/complex fitting method. Magn Reson Med 2012;67(3):638–644.
53. Yu H, Shimakawa A, Hines CDG, et al. Combination of complex-based and magnitude-based multiecho water-fat separation for accurate quantification of fat-fraction. Magn Reson Med 2011;66(1):199–206.
54. Colgan TJ, Hernando D, Sharma SD, Reeder SB. The effects of concomitant gradients on chemical shift encoded MRI. Magn Reson Med 2017;78(2):730–738.
55. Hernando D, Sharma SD, Kramer H, Reeder SB. On the confounding effect of temperature on chemical shift-encoded fat quantification. Magn Reson Med 2014;72(2):464–470.
56. Kühn JP, Hernando D, Mensel B, et al. Quantitative chemical shift-encoded MRI is an accurate method to quantify hepatic steatosis. J Magn Reson Imaging 2014;39(6):1494–1501.
57. Yokoo T, Serai SD, Pirasteh A, et al. Linearity, bias, and precision of hepatic proton density fat fraction measurements by using MR imaging: A meta-analysis. Radiology 2018;286(2):486–498.
58. Idilman IS, Keskin O, Celik A, et al. A comparison of liver fat content as determined by magnetic resonance imaging-proton density fat fraction and MRS versus liver histology in non-alcoholic fatty liver disease. Acta Radiol 2016;57(3):271–278.
59. Hernando D, Sharma SD, Aliyari Ghasabeh M, et al. Multisite, multivendor validation of the accuracy and reproducibility of proton-density fat-fraction quantification at 1.5T and 3T using a fat-water phantom. Magn Reson Med 2017;77(4):1516–1524.
60. Bernard CP, Liney GP, Manton DJ, Turnbull LW, Langton CM. Comparison of fat quantification methods: a phantom study at 3.0T. J Magn Reson Imaging 2008;27(1):192–197.
61. Bush EC, Gifford A, Coolbaugh CL, Towse TF, Damon BM, Welch EB. Fat-water phantoms for magnetic resonance imaging validation: A flexible and scalable protocol. J Vis Exp 2018;2018(139):9.
62. Navaratna R, Zhao R, Colgan TJ, et al. Temperature-corrected proton density fat fraction estimation using chemical shift-encoded MRI in phantoms. Magn Reson Med 2021;86(1):69–81.
63. Qayyum A. MR spectroscopy of the liver: principles and clinical applications. RadioGraphics 2009;29(6):1653–1664.
64. Hamilton G, Yokoo T, Bydder M, et al. In vivo characterization of the liver fat ^{1}H MR spectrum. NMR Biomed 2011;24(7):784–790.
65. Hamilton G, Middleton MS, Hooker JC, et al. In vivo breath-hold (1) H MRS simultaneous estimation of liver proton density fat fraction, and T1 and T2 of water and fat, with a multi-TR, multi-TE sequence. J Magn Reson Imaging 2015;42(6):1538–1543.
66. Hamilton G, Middleton MS, Bydder M, et al. Effect of PRESS and STEAM sequences on magnetic resonance spectroscopic liver fat quantification. J Magn Reson Imaging 2009;30(1):145–152.
67. Lee H, Jun DW, Kang BK, et al. Estimating of hepatic fat amount using MRI proton density fat fraction in a real practice setting. Medicine (Baltimore) 2017;96(33):e7778.
68. ter Voert EGW, Heijmen L, van Laarhoven HWM, Heerschap A. In vivo magnetic resonance spectroscopy of liver tumors and metastases. World J Gastroenterol 2011;17(47):5133–5149.
69. Tyagi A, Yeganeh O, Levin Y, et al. Intra- and inter-examination repeatability of magnetic resonance spectroscopy, magnitude-based MRI, and complex-based MRI for estimation of hepatic proton density fat fraction in overweight and obese children and adults. Abdom Imaging 2015;40(8):3070–3077.
70. Meisamy S, Hines CDG, Hamilton G, et al. Quantification of hepatic steatosis with T1-independent, T2-corrected MR imaging with spectral modeling of fat: blinded comparison with MR spectroscopy. Radiology 2011;258(3):767–775.
71. Yu H, Reeder SB, Shimakawa A, Brittain JH, Pelc NJ. Field map estimation with a region growing scheme for iterative 3-point water-fat decomposition. Magn Reson Med 2005;54(4):1032–1039.
72. Hernando D, Haldar JP, Sutton BP, Ma J, Kellman P, Liang ZP. Joint estimation of water/fat images and field inhomogeneity map. Magn Reson Med 2008;59(3):571–580.
73. Hines CDG, Yu H, Shimakawa A, McKenzie CA, Brittain JH, Reeder SB. T1 independent, T2* corrected MRI with accurate spectral modeling for quantification of fat: validation in a fat-water-SPIO phantom. J Magn Reson Imaging 2009;30(5):1215–1222.

74. Hines CDG, Agni R, Roen C, et al. Validation of MRI biomarkers of hepatic steatosis in the presence of iron overload in the ob/ob mouse. J Magn Reson Imaging 2012;35(4):844–851.
75. Hines CDG, Yu H, Shimakawa A, et al. Quantification of hepatic steatosis with 3-T MR imaging: validation in ob/ob mice. Radiology 2010;254(1):119–128.
76. Bannas P, Kramer H, Hernando D, et al. Quantitative magnetic resonance imaging of hepatic steatosis: Validation in ex vivo human livers. Hepatology 2015;62(5):1444–1455.
77. Idilman IS, Aniktar H, Idilman R, et al. Hepatic steatosis: quantification by proton density fat fraction with MR imaging versus liver biopsy. Radiology 2013;267(3):767–775.
78. Noureddin M, Lam J, Peterson MR, et al. Utility of magnetic resonance imaging versus histology for quantifying changes in liver fat in nonalcoholic fatty liver disease trials. Hepatology 2013;58(6):1930–1940.
79. Tang A, Tan J, Sun M, et al. Nonalcoholic fatty liver disease: MR imaging of liver proton density fat fraction to assess hepatic steatosis. Radiology 2013;267(2):422–431.
80. Artz NS, Haufe WM, Hooker CA, et al. Reproducibility of MR-based liver fat quantification across field strength: Same-day comparison between 1.5T and 3T in obese subjects. J Magn Reson Imaging 2015;42(3):811–817.
81. Pooler BD, Hernando D, Reeder SB. Clinical implementation of a focused MRI protocol for hepatic fat and iron quantification. AJR Am J Roentgenol 2019;213(1):90–95.
82. Kim B, Kim SY, Kim KW, et al. MRI in donor candidates for living donor liver transplant: Technical and practical considerations. J Magn Reson Imaging 2018;48(6):1453–1467.
83. Hernando D, Levin YS, Sirlin CB, Reeder SB. Quantification of liver iron with MRI: state of the art and remaining challenges. J Magn Reson Imaging 2014;40(5):1003–1021.
84. Radiology question for the week of April 1, 2019. Medlearn Media web site. https://www.medlearnmedia.com/question-of-the-week/radiology/radiology-question-for-the-week-of-april-1-2019/. Published online April 1, 2019. Accessed September 2, 2021.
85. Guo Z, Blake GM, Li K, et al. Liver fat content measurement with quantitative CT validated against MRI proton density fat fraction: A prospective study of 400 healthy volunteers. Radiology 2020;294(1):89–97.
86. Vu KN, Gilbert G, Chalut M, Chagnon M, Chartrand G, Tang A. MRI-determined liver proton density fat fraction, with MRS validation: Comparison of regions of interest sampling methods in patients with type 2 diabetes. J Magn Reson Imaging 2016;43(5):1090–1099.
87. Campo CA, Hernando D, Schubert T, Bookwalter CA, Pay AJV, Reeder SB. Standardized Approach for ROI-Based Measurements of Proton Density Fat Fraction and R2* in the Liver. AJR Am J Roentgenol 2017;209(3):592–603.
88. Qayyum A, Nystrom M, Noworolski SM, Chu P, Mohanty A, Merriman R. MRI steatosis grading: development and initial validation of a color mapping system. AJR Am J Roentgenol 2012;198(3):582–588.
89. Graffy PM, Sandfort V, Summers RM, Pickhardt PJ. Automated Liver Fat Quantification at Nonenhanced Abdominal CT for Population-based Steatosis Assessment. Radiology 2019;293(2):334–342.
90. Huo Y, Terry JG, Wang J, etal. Fully automatic liver attenuation estimation combing CNN segmentation and morphological operations. Med Phys 2019;46(8):3508–3519.
91. Jirapatnakul A, Reeves AP, Lewis S, et al. Automated measurement of liver attenuation to identify moderate-to-severe hepatic steatosis from chest CT scans. Eur J Radiol 2020;122:108723.
92. Kullberg J, Hedström A, Brandberg J, et al. Automated analysis of liver fat, muscle and adipose tissue distribution from CT suitable for large-scale studies. Sci Rep 2017;7(1):10425.
93. Wang K, Mamidipalli A, Retson T, et al. Automated CT and MRI Liver Segmentation and Biometry Using a Generalized Convolutional Neural Network. Radiol Artif Intell 2019;1(2):180022.
94. Stocker D, Bashir MR, Kannengiesser SAR, Reiner CS. Accuracy of Automated Liver Contouring, Fat Fraction, and R2* Measurement on Gradient Multiecho Magnetic Resonance Images. J Comput Assist Tomogr 2018;42(5):697–706.
95. Yan HM, Xia MF, Wang Y, et al. Efficacy of berberine in patients with nonalcoholic fatty liver disease. PLoS One 2015;10(8):e0134172.
96. Roberts NT, Hernando D, Holmes JH, Wiens CN, Reeder SB. Noise properties of proton density fat fraction estimated using chemical shift-encoded MRI. Magn Reson Med 2018;80(2):685–695.
97. Luo H, Zhu A, Wiens CN, et al. Free-breathing liver fat and R*2 quantification using motion-corrected averaging based on a nonlocal means algorithm. Magn Reson Med 2021;85(2):653–666.
98. Motosugi U, Hernando D, Bannas P, et al. Quantification of liver fat with respiratory-gated quantitative chemical shift encoded MRI. J Magn Reson Imaging 2015;42(5):1241–1248.
99. Armstrong T, Dregely I, Stemmer A, et al. Free-breathing liver fat quantification using a multiecho 3D stack-of-radial technique. Magn Reson Med 2018;79(1):370–382.
100. Zhao R, Zhang Y, Wang X, et al. Motion-robust, high-SNR liver fat quantification using a 2D sequential acquisition with a variable flip angle approach. Magn Reson Med 2020;84(4):2004–2017.
101. Armstrong T, Ly KV, Murthy S, et al. Free-breathing quantification of hepatic fat in healthy children and children with nonalcoholic fatty liver disease using a multi-echo 3-D stack-of-radial MRI technique. Pediatr Radiol 2018;48(7):941–953.
102. Pooler BD, Hernando D, Ruby JA, Ishii H, Shimakawa A, Reeder SB. Validation of a motion-robust 2D sequential technique for quantification of hepatic proton density fat fraction during free breathing. J Magn Reson Imaging 2018;48(6):1578–1585.
103. Schneider M, Benkert T, Solomon E, et al. Free-breathing fat and R_2* quantification in the liver using a stack-of-stars multi-echo acquisition with respiratory-resolved model-based reconstruction. Magn Reson Med 2020;84(5):2592–2605.
104. Mann LW, Higgins DM, Peters CN, et al. Accelerating MR imaging liver steatosis measurement using combined compressed sensing and parallel imaging: A quantitative evaluation. Radiology 2016;278(1):247–256.
105. Jaubert O, Arrieta C, Cruz G, et al. Multi-parametric liver tissue characterization using MR fingerprinting: Simultaneous T_1, T_2, T_2*, and fat fraction mapping. Magn Reson Med 2020;84(5):2625–2635.
106. Szczepaniak LS, Nurenberg P, Leonard D, et al. Magnetic resonance spectroscopy to measure hepatic triglyceride content: prevalence of hepatic steatosis in the general population. Am J Physiol Endocrinol Metab 2005;288(2):E462–E468.
107. Cunha GM, Thai TT, Hamilton G, et al. Accuracy of common proton density fat fraction thresholds for magnitude- and complex-based chemical shift-encoded MRI for assessing hepatic steatosis in patients with obesity. Abdom Radiol (NY) 2020;45(3):661–671.
108. Rehm JL, Wolfgram PM, Hernando D, Eickhoff JC, Allen DB, Reeder SB. Proton density fat-fraction is an accurate biomarker of hepatic steatosis in adolescent girls and young women. Eur Radiol 2015;25(10):2921–2930.
109. Di Martino M, Pacifico L, Bezzi M, et al. Comparison of magnetic resonance spectroscopy, proton density fat fraction and histological analysis in the quantification of liver steatosis in children and adolescents. World J Gastroenterol 2016;22(39):8812–8819.
110. Patel J, Bettencourt R, Cui J, et al. Association of noninvasive quantitative decline in liver fat content on MRI with histologic response in nonalcoholic steatohepatitis. Therap Adv Gastroenterol 2016;9(5):692–701.
111. Pickhardt PJ, Graffy PM, Zea R, et al. Automated CT biomarkers for opportunistic prediction of future cardiovascular events and mortality in an asymptomatic screening population: a retrospective cohort study. Lancet Digit Health 2020;2(4):e192–e200.
112. Chen X, Li K, Yip R, et al. Hepatic steatosis in participants in a program of low-dose CT screening for lung cancer. Eur J Radiol 2017;94:174–179.
113. Le TA, Chen J, Changchien C, et al. Effect of colesevelam on liver fat quantified by magnetic resonance in nonalcoholic steatohepatitis: a randomized controlled trial. Hepatology 2012;56(3):922–932.
114. Cui J, Philo L, Nguyen P, et al. Sitagliptin vs. placebo for non-alcoholic fatty liver disease: A randomized controlled trial. J Hepatol 2016;65(2):369–376.
115. Jayakumar S, Middleton MS, Lawitz EJ, et al. Longitudinal correlations between MRE, MRI-PDFF, and liver histology in patients with non-alcoholic steatohepatitis: Analysis of data from a phase II trial of selonsertib. J Hepatol 2019;70(1):133–141.
116. Kooby DA, Fong Y, Suriawinata A, et al. Impact of steatosis on perioperative outcome following hepatic resection. J Gastrointest Surg 2003;7(8):1034–1044.
117. Chu MJJ, Dare AJ, Phillips ARJ, Bartlett ASJR. Donor Hepatic Steatosis and Outcome After Liver Transplantation: a Systematic Review. J Gastrointest Surg 2015;19(9):1713–1724.